Labyrinthic standard non-twist map

2011 J. Phys. A: Math. Theor. 44 045102

(http://iopscience.iop.org/1751-8121/44/4/045102)

IOP Publishing Journal of Physics A: Mathematical and Theoretical

J. Phys. A: Math. Theor. **44** (2011) 045102 (9pp) doi:10.1088/1751-8113/44/4/045102

Labyrinthic standard non-twist map

C G L Martins[1,3], R Egydio de Carvalho[1,4], I L Caldas[2] and M Roberto[3]

[1] Universidade Estadual Paulista-UNESP, 13506-900 Rio Claro, SP Brazil
[2] Instituto Tecnológico da Aeronáutica-ITA, 12228-900 São José dos Campos, SP Brazil
[3] Universidade de São Paulo-USP, 05315-970 São Paulo, SP Brazil

E-mail: carolinegameiro@gmail.com, regydio@rc.unesp.br, ibere@if.usp.br and marisar@ita.br

Received 30 August 2010
Published 22 December 2010
Online at stacks.iop.org/JPhysA/44/045102

Abstract

We introduce the labyrinthic standard non-twist map, which is a modified non-twist standard map with an additional perturbation which is a period multiple of the original perturbation period. In phase space this map can present several sets of invariant meandering curves due to the reconnection process of isochrones resonances. Inside each meander set we can find a non-twist invariant curve called the shearless curve, with an extreme rotation number, which generates a wide stickiness effect in phase space when it is broken. The birth/break of these shearless curves, as well as their effects on the dynamical transport are studied, showing the formation of many transport barriers in the system.

(Some figures in this article are in colour only in the electronic version)

1. Introduction

Non-twist maps arise naturally in the study of Hamiltonian systems which describe, for example, particle transport and magnetic field lines in plasma physics [1, 2], flows in fluid dynamics [3, 4], and orbits in celestial mechanics [5]. Apart from their importance in physics, non-twist maps are also of mathematical interest because KAM and Poincare–Birkhoff theorems are not obeyed around the non-twist region [6–11].

In this paper we consider a new discrete area-preserving map that violates the so-called twist condition. The labyrinthic standard non-twist map proposed in this work can be very useful as a model for the understanding of new dynamic features of non-twist models, as transport and transition to global chaos.

Several area-preserving maps in physics can be described in the following form:

$$\begin{aligned} x_{n+1} &= x_n + \alpha(y_{n+1}) + \varepsilon g(x_n, y_{n+1}) \\ y_{n+1} &= y_n + \varepsilon f(x_n, y_{n+1}) \end{aligned} \tag{1}$$

[4] Author to whom any correspondence should be addressed.

where the area preservation condition reads as

$$\frac{\partial f}{\partial x_n} + \frac{\partial g}{\partial y_{n+1}} = 0. \tag{2}$$

The map (1) is usually originated from delta kicked Hamiltonian systems such as

$$H(x, y, t) = H_0(y) + \varepsilon H_1(x, y, t) \tag{3}$$

where H_0 is the unperturbed Hamiltonian, H_1 is the perturbation and ε is the control parameter. The functions f and g, which appear in equation (2), when we deal with a Hamiltonian formulation, are associated with the perturbation H_1 and can be written in the form,

$$f(x, y) = \frac{\partial H_1(x, y)}{\partial x}, \qquad g(x, y) = \frac{\partial H_1(x, y)}{\partial y}. \tag{4}$$

The function $\alpha(y) = \frac{\partial H_0(y)}{\partial y}$, associated with $\alpha(y_{n+1})$ in equation (1), is the frequency of the unperturbed Hamiltonian, in other words, it is the rotation number for the system without any perturbation.

The twist condition for maps is

$$\frac{\partial x_{n+1}}{\partial y_n} \neq 0 \tag{5}$$

and it corresponds to the non-degeneracy condition for the Hamiltonian flux:

$$\frac{\partial^2 H_0}{\partial y^2} \neq 0. \tag{6}$$

The violation of the twist condition, or the non-degeneracy condition, is responsible for the appearance of isochronous resonances [12, 13] and leads to non-twist maps or degenerated Hamiltonians. These resonances can interact and reconnect producing a local, but wide, topological rearrangement. After the reconnection, a region with meandering tori appears which corresponds to a transport barrier in phase space [6, 14]. After the destruction of the last meandering torus, called shearless torus [6], this region still plays a very important role because there are many small islands causing a strong stickiness effect around it [15]. Then, for some physical systems in which it is assumed that transport barriers are important, the meandering tori stand out as being a powerful tool [3, 6, 16, 17].

2. Labyrinthic standard non-twist map and degenerated meandering tori

In order to derive the new map, which brings all characteristics of the usual non-twist maps, but with a plenty of regions with meanders, we will start with the Hamiltonian

$$H(x, y, t) = \left[a\left(y - \frac{y^3}{3}\right)\right] + b\left\{\frac{1}{2\pi}\cos(2\pi x)\sum_{n=-\infty}^{\infty}\delta(t - n)\right\}. \tag{7}$$

The term in brackets is the unperturbed Hamiltonian, which will introduce two isochronous resonances and the term in curly brackets is the kicked delta perturbation.

According to equation (4) we can define the functions $f(x, y)$, $g(x, y)$ and $\alpha(y)$, respectively as, $f(x, y) = -\sin(2\pi x)$, $g(x, y) = 0$ and $\alpha(y) = a(1 - y^2)$ which lead to the well-known standard non-twist map [6]:

$$\begin{aligned} x_{n+1} &= x_n + a\left(1 - y_{n+1}^2\right) \\ y_{n+1} &= y_n - b\sin(2\pi x_n) \end{aligned} \tag{8}$$

where a and b are the control parameters and x has period 1.

Now, we introduce another perturbation in equation (7), similar to the term in curly brackets, but with η in the argument of the periodic function, where η is an integer number. Hence, the new Hamiltonian is given by

$$\mathrm{H}(x, y, t) = \left[a\left(y - \frac{y^3}{3}\right)\right] + b\left\{\frac{1}{2\pi}\cos(2\pi x)\sum_{n=-\infty}^{\infty}\delta(t-n) + \frac{1}{\eta 2\pi}\cos(\eta 2\pi x)\sum_{n=-\infty}^{\infty}\delta(t-n)\right\}. \tag{9}$$

The corresponding discrete map derived from the Hamiltonian above, we call *labyrinthic standard non-twist map (LSNM)*,

$$\begin{aligned} x_{n+1} &= x_n + a(1 - y_{n+1}^2) \\ y_{n+1} &= y_n - b\sin(2\pi x_n) - b\sin(\eta 2\pi x_n). \end{aligned} \tag{10}$$

For $b \neq 0$, the rotation number profile is modified by the perturbation and has to be calculated for each orbit, with initial conditions $(x_0,\ y_0)$. It is defined as the limit, $\alpha(x_0, y_0) = \lim_{n\to\infty} \frac{\Delta x_n}{n}$ [14].

The terminology labyrinthic found in our LSNM was first introduced by Simó [18], and it refers to the shape of the regions with meandering tori, named labyrinthic curves; indeed they look like a path on a maze, where the walls of the maze are the manifolds of the hyperbolic fixed points.

The new perturbation, in equation (10), superposes with the first one and the parameter η is responsible for the bifurcations of the fixed points of the main island chains creating an interesting topological effect.

Figure 1 shows the phase space of the LSNM from equation (10) for four different values of η. In figure 1(*a*), $\eta = 1$, the new map recovers the dynamics of the well-known standard non-twist map, with two isochronous island chains, each one of them with one hyperbolic fixed point and one elliptic fixed point representing a resonance with mode (1:1) [17]. Figure 1(*b*) has $\eta = 2$ and shows the first bifurcation, the fixed points located at $x = 0.5$ bifurcated. The elliptic fixed point of the upper island chain bifurcated in one hyperbolic and two elliptic fixed points and the opposite has occurred for the lower island chain, the hyperbolic fixed point bifurcated in one elliptic and two hyperbolic fixed points. The number of stable fixed points in each island chain is equal to the value of the parameter η, the same happens to the number of instable fixed points. We can note that the bifurcation of the elliptic fixed point of the upper island chain in figure 1(*b*) is characterized by a pitchfork bifurcation and the bifurcation of the hyperbolic fixed point of the lower island chain is characterized by an inverse pitchfork bifurcation. As we increase the parameter η the same bifurcations occur, always for the fixed points located at $x = 0.5$, as we can see in figure 1(*c*), which has $\eta = 3$, and in figure 1(*d*), which has $\eta = 4$.

As previously mentioned, a remarkable characteristic of non-twist maps is the occurrence of a region with meandering tori, which can be found in the region surrounding the islands after their overlapping.

In the new map, LSNM, a new effect occurs due to the presence of the second perturbation. The new manifolds, associated with the hyperbolic fixed points that appeared from the bifurcations, can also start a reconnection process as the intensity of the control parameter b is increased.

In the plots of figure 2 we fixed $\eta = 4$ and $a = 1.006$. In figures 2(*a*), (*c*), (*e*) and (*g*) we vary b to investigate the topology of the phase space. In figures 2(*b*), (*d*), (*f*) and (*h*) is shown the rotation number as a function of y for initial conditions along a line with $x_{\text{initial}} = 0.5$. In

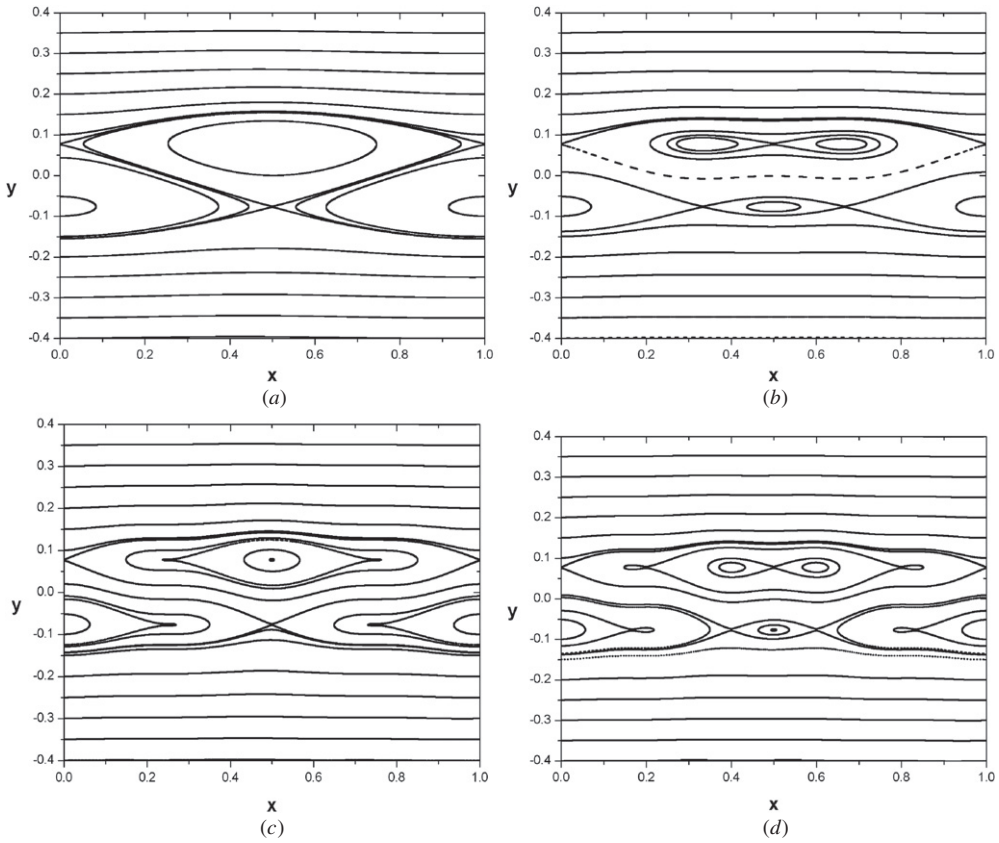

Figure 1. Bifurcations for the labyrinthic standard non-twist map from equation (10) with $a = 1.006$ and $b = 0.001$ for (*a*) $\eta = 1$; (*b*) $\eta = 2$; (*c*) $\eta = 3$; (*d*) $\eta = 4$.

figure 2(*a*), there are two independent resonance structures separated by some meandering curves in pink, and figure 2(*b*) shows the rotation number for this case. As we can see there is a line with $\alpha = 1$ representing the original resonant mode (1:1), (see figure 1(*a*)), and there is a global maximum indicating a shearless torus with $\mathrm{d}\alpha(x, y)/\mathrm{d}y = 0$, between the two structures and inside in pink. In figure 2(*c*), we see the first reconnection and a first region of meandering tori blue. The first region with meanders can be seen in figure 2(*d*), which presents a local minimum for the rotation number. It represents a shearless torus in blue. Figure 2(*e*) shows the second reconnection and a second region with meandering tori in red. It can be noted in figure 2(*f*) the birth of a second local minimum for the rotation number, representing a second shearless torus in phase space. Finally, in figure 2(*g*) the last reconnection took place and a third region with meandering tori is shown in green. The last local minimum for the rotation number appears in figure 2(*h*). We define these sets of meandering tori, from all the different colored regions, as *degenerated meandering tori (DMT)*, due to the fact that they emerge from an only pair of isochronous resonances (1:1). We emphasize that the big hill, associated with the shearless, which was present in figure 2(*b*) disappeared due to the overlap of the resonances. New shearless tori appear as a consequence of this overlapping.

In all plots of figure 2, the parameter b has been slightly increased to show the DMT formations and the chaos surrounding the hyperbolic fixed points which is too tiny to be noticed. We also point out that the number of regions with DMT is equal to $(\eta - 1)$ which, in

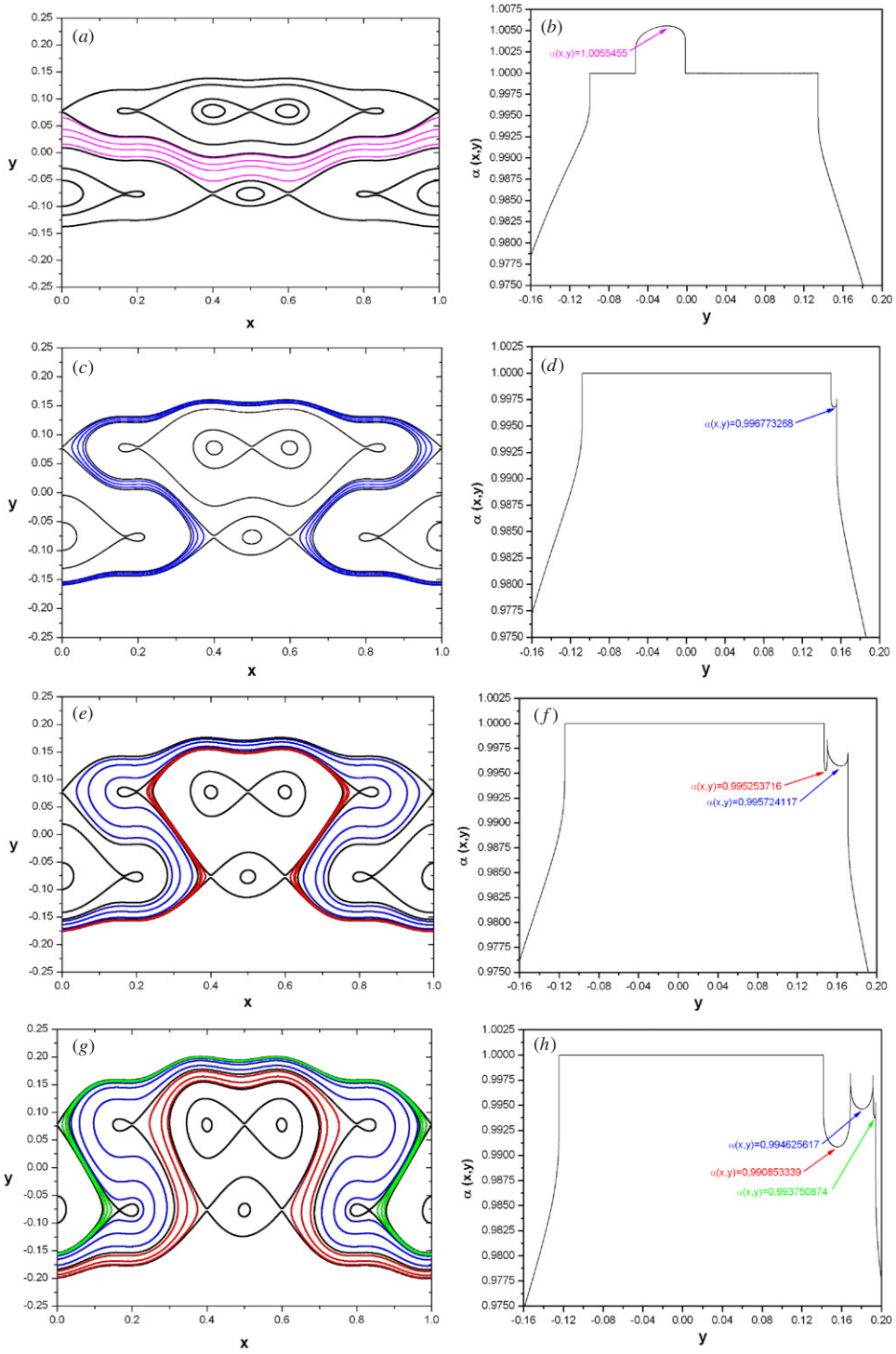

Figure 2. Reconnection process of island chains and their rotation numbers, calculated for initial conditions along $x = 0.5$, for the LSNM from equation (10) with $\eta = 4$ and $a = 1.006$ for (a) and (b) $b = 0.001$; (c) and (d) $b = 0.002$; (e) and (f) $b = 0.003$; (g) and (h) $b = 0.005$.

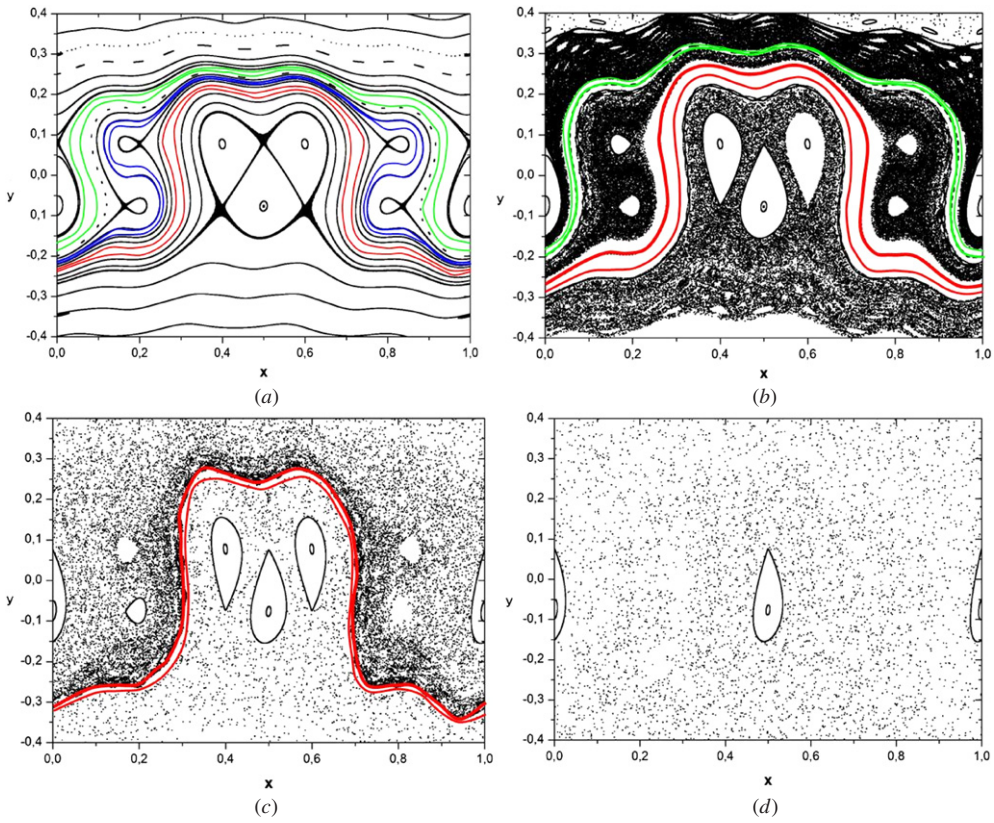

Figure 3. Gradual destruction of the meandering tori regions of the labyrinthic standard non-twist map from equation (10) with $\eta = 4$ and $a = 1.006$ for (*a*) $b = 0.015$; (*b*) $b = 0.028$; (c) $b = 0.043$; (d) $b = 0.059$.

the cases of figure 2, is equal to 3. These regions are plotted with different colors to emphasize the three different regions of DMT and their respective shearless tori.

3. Robustness of the degenerated meandering tori

Another important aspect of the meandering curves is connected with their rotation number. In [6] the authors have shown that the region with meanders has periodic orbits that can undergo local reconnections and bifurcations. They have shown numerically that a reconnection process occurs locally inside the region with meanders and they called this kind of reconnection as 'second-order reconnection'. As the perturbation parameter increases, other reconnections happen inside the meanders structures and consequently the order of the reconnections also increases. This scenario produces, after the breakup of the shearless torus, a strong stickiness in the meanders region which constitutes an important transport barrier [4, 6, 14, 15].

In figures 3 we present plots for four values of the control parameter in order to show the enlargement of the stickiness area and also to evaluate the robustness of each region of meandering tori. In figure 3(*a*), $b = 0.015$, which is similar to figure 2(*g*), a thin layer of chaos can be seen around the hyperbolic fixed points. We also observe three colored regions with meandering tori. In figure 3(*b*), $b = 0.028$, we observe that the region with blue meandering

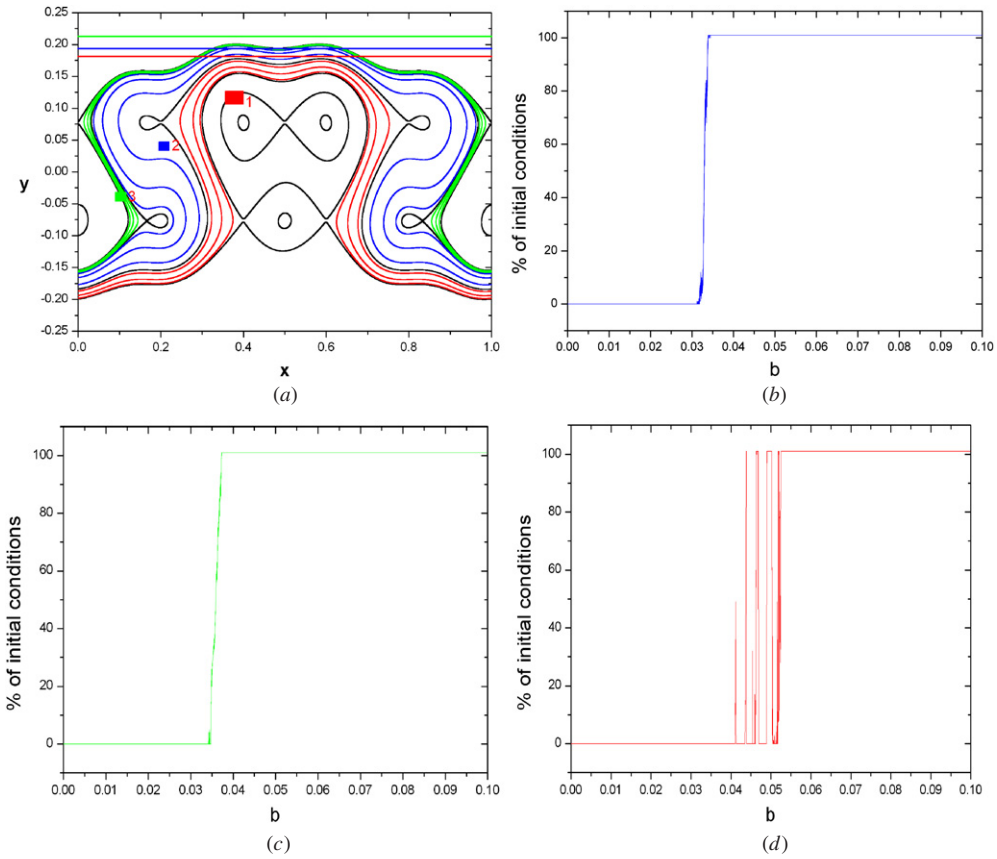

Figure 4. Transport along the phase space, with $\eta = 4$ and $a = 1.006$; (*a*) Generic scenario used to study the robustness of meandering tori from different colors (*b*) Percentage of orbits that cross the blue region. (*c*) Percentage of orbits that cross the green region. (*d*) Percentage of orbits that cross the red region.

tori was destroyed, but the local chaotic sea is confined by the other two regions of meandering tori. Figure 3(*c*), $b = 0.043$, presents the most robust region with meandering tori, which is marked in red color, any orbit below the red tori is blocked and it does not attain the region above these curves. We noted that the green meandering tori are already destroyed for this case. We point out that in the region related to the color blue, some initial conditions remain trapped, even after the destruction of the blue shearless torus, showing a stickiness effect in phase space as can be seen in figure 3(*b*). In figure 3(*d*), $b = 0.059$, the perturbation is so strong that the phase space does not present anymore meandering tori.

The order of creation of the meanders regions is not the same order of their destruction. The first region created by the reconnection was the blue one, the second was the red one and the last region was the green one. As we increase the parameter b, the sequence of destruction is blue, green and finally the red region. From our results, we can relate the frequency of the angular variable x with the stability of the region. We observed that the region, which has the shearless torus with the lowest rotation number is the more robust to be broken by the perturbation, i.e. as smaller the rotation number the more robust the shearless torus.

The same characterization of the robustness of the DMT can be observed quantitatively through the evaluation of the transport along the phase space. In figure 4(*a*) we show a

representative phase space, with the three regions of meandering tori, where we have defined three colored boxes with 100 initial conditions in each one and also three reference lines with the corresponding colors. We have varied the control parameter b in the range [0.0; 0.1] and we analyzed how many initial conditions, departing from a specific box, attained the corresponding line after 2×10^4 iterations. In figure 4(b) we see the behavior of the blue region with meandering tori. This is the first destroyed region with the increase of the perturbation parameter b. Around the value $b = 0.035$ all meanders tori are completely destroyed and 100% of the initial conditions crossed the corresponding barrier (blue) and attained the corresponding reference line. Figure 4(c) shows the second region (green) of meandering tori destroyed in phase space. We can see that around $b = 0.040$, the barrier is already completely destroyed. Finally, in figure 4(d) we see the destruction of the strongest meanders region, the red one, which has the most robust shearless torus. The destruction of the red region occurs around $b = 0.055$.

Looking at the structure of the map in equation (10), it is easy to note that we can introduce as many barriers as we want depending only on the parameter η, and this is the main characteristic of the labyrinthic standard non-twist map. This creation of transport barriers may be useful in physics, as, for example, to improve the plasma confinement in tokamaks [7, 16, 17, 20–24].

4. Final remarks and conclusion

In this paper we introduced a modification in the standard non-twist map through the superposition of two correlated periodic perturbations in such way that the ratio of their periods is always an integer parameter. The new perturbation interacts with the first one and a new topological effect occurs, i.e. the creation of many reconnections processes resulting on several meanders regions, each of them with their own shearless torus. We have called the new map a labyrinthic standard non-twist map (LSNM) and we studied the birth/break up of the different meanders regions in the system.

The parameter η is responsible for the bifurcation mechanism which creates all the reconnections. The number of meanders regions with shearless tori created by them is equal to $(\eta - 1)$, then, we can have as many dynamical barriers as we want in the system. Based on our numerical results, we conjecture that the strongest shearless torus in the system is the one with the lowest rotation number, at least when there are only two isochronous resonances before the reconnection.

Acknowledgments

The authors thank the scientific Brazilian agencies FAPESP, CNPQ and CAPES for financial support, and the Univ Estadual Paulista (UNESP) for the opportunity to develop this work.

References

[1] Balescu R 1998 *Phys. Rev.* E **58** 3781
[2] Oda G A and Caldas I L 1995 *Chaos Solitons Fractals* **5** 15
[3] Weiss J B 1991 *Phys. Fluids* A **3** 1379
[4] del-Castillo-Negrete D and Morrison P J 1993 *Phys. Fluids* A **5** 948
[5] Munteanu A, García-Berro E, José J and Petrisor E 2002 *Chaos* **12** 332
[6] Wurm A, Apte A and Morrison P J 2004 *Braz. J. Phys.* **34** 1700
[7] Morrison P J 2000 *Phys. Plasma* **7** 2279
[8] Meiss J D 1992 *Rev. Mod. Phys.* **64** 795

[9] Martins C G L, Egydio de Carvalho R, Caldas I L and Roberto M 2010 *J. Phys. A: Math. Theor.* **43** 175501
[10] Martins C G L, Marcus F A, Caldas I L and Egydio de Carvalho R 2010 *Physica* **A** at press (doi:10.1016/j.physa.2010.11.025)
[11] Martins C G L, Egydio de Carvalho R, Caldas I L and Roberto M 2010 *J. Phys: Conf. Ser.* **246** 012005
[12] Egydio de Carvalho R and Ozório de Almeida A M 1992 *Phys. Lett* A **162** 457
[13] Egydio de Carvalho R 1993 *Nonlinearity* **6** 973
[14] Wurm A, Apte A, Fuchss K and Morrison P J 2005 *Chaos* **15** 023108
[15] Szezech J D Jr, Caldas I L, Lopes S R, Viana R L and Morrison P J 2009 *Chaos* **19** 043108
[16] Roberto M, da Silva E C, Caldas I L and Viana R L 2004 *Phys. Plasma* **11** 214
[17] Roberto M, da Silva E C, Caldas I L and Viana R L 2004 *Physica* A **342** 363
[18] Simó C 1998 *Reg. Chaotic Dyn.* **3** 180
[19] del-Castillo-Negrete D, Greene J M and Morrison P J 1997 *Physica* D **100** 311
[20] Horton W 1999 *Rev. Mod. Phys.* **71** 735
[21] Finken K H *et al* 2008 *Nucl. Fusion* **48** 024001
[22] Levinton F M *et al* 1995 *Phys. Rev. Lett.* **75** 4417
[23] Kucinski M Y and Caldas I L 1987 *Z. Natuforsch.* A **42** 1124
[24] Portela J S E, Caldas I L and Viana R L 2008 *Eur. Phys. J. Spec. Top.* **165** 195